Journal of
Synchrotron Radiation

ISSN 0909-0495

Received 14 September 2009
Accepted 5 February 2010

Coherence and wavefront characterization of Si-111 monochromators using double-grating interferometry

Ana Diaz,[a,b]*‡ Cristian Mocuta,[a]¶ Julian Stangl,[b] Mario Keplinger,[b] Timm Weitkamp,[a] Franz Pfeiffer,[c,d]§ Christian David,[c] Till H. Metzger[a] and Günther Bauer[b]

[a]European Synchrotron Radiation Facility, 6 rue Jules Horowitz, BP 220, 38043 Grenoble Cedex, France, [b]Institute of Semiconductor and Solid State Physics, Johannes Kepler Universität, Altenbergerstrasse 69, A-4040 Linz, Austria, [c]Paul Scherrer Institut, 5232 Villigen PSI, Switzerland, and [d]Ecole Polytechnique Fédérale de Lausanne, 1015 Lausanne, Switzerland.
E-mail: ana.diaz@psi.ch

A study of the coherence and wavefront properties of a pseudo-channel-cut monochromator in comparison with a double-crystal monochromator is presented. Using a double-grating interferometer designed for the hard X-ray regime, the complex coherence factor was measured and the wavefront distortions at the sample position were analyzed. A transverse coherence length was found in the vertical direction that was a factor of two larger for the channel-cut monochromator owing to its higher mechanical stability. The wavefront distortions after different optical elements in the beam, such as monochromators and mirrors, were also quantified. This work is particularly relevant for coherent diffraction imaging experiments with synchrotron sources.

Keywords: X-rays; coherence; interferometry; wavefront characterization.

1. Introduction

In recent years the number of experiments exploiting the coherence of synchrotron sources has steadily risen. As an example, coherent diffraction X-ray imaging (CDI) relies on the measurement of oversampled diffraction patterns from an object in order to image it using iterative phase-retrieval algorithms (Miao *et al.*, 1999; Williams *et al.*, 2003; Pfeifer *et al.*, 2006; Thibault *et al.*, 2008; Abbey *et al.*, 2008). Also, in X-ray photon correlation spectroscopy (XPCS), time-dependent coherent speckle from a system is recorded as a function of time in order to study its dynamics (Dierker *et al.*, 1995; Gutt *et al.*, 2003, 2007; Shpyrko *et al.*, 2007). In all these studies one can only use a fraction of the beam which is as large as the so-called coherence volume inherent to the X-ray source size and to the spectral bandwidth of the radiation. However, the optical elements between the source and the sample, including the necessary monochromator, can drastically change the coherence properties of the X-ray beam by introducing vibrations and wavefront distortions, resulting in difficulties in retrieving the phase in coherent diffraction experiments (Vartanyants & Robinson, 2001, 2003; Williams *et al.*, 2007). For this reason, the coherence characterization of X-rays and the choice of appropriate optical elements in a beamline are crucial in this kind of experiment.

Many methods have been developed in order to quantify the transverse coherence length at synchrotron sources (Kohn *et al.*, 2000; Guigay *et al.*, 2004; Leitenberger *et al.*, 2004). Some of them serve for the measurement of the complex coherence factor (Lin *et al.*, 2003; Pfeiffer *et al.*, 2005), the knowledge of which is necessary in CDI when partial coherence effects occur. In these studies the measured spatial coherence length is usually smaller than that expected from the beamline parameters. These deviations are usually attributed to imperfections in the optical elements of the beamline. However, a systematic study comparing the coherence properties of the X-ray beam after different optical elements is needed in order to choose the most convenient elements in coherent scattering experiments.

In this article we present a study of the coherence and wavefront properties of a synchrotron X-ray beam after passing through different optical elements such as monochromators and mirrors in both transverse directions (vertical and horizontal). Using a double-grating interferometer (Pfeiffer *et al.*, 2005), we measured the complex coherence factor and local wavefront radius of curvature at the sample position of a synchrotron beamline. We show that a pseudo-channel-cut monochromator can provide a transverse coher-

‡ Present address: Paul Scherrer Institut, 5232 Villigen PSI, Switzerland.
¶ Present address: Synchrotron Soleil, L'Orme des Merisiers, St Aubin, BP 48, 91192 Gif-Sur-Yvette, France.
§ Present address: Department-Physik E17, Technische Universität München, 84758 Garching, Germany.

ence length twice as large as a conventional high-flux double-crystal monochromator, while not presenting stronger wavefront distortions. We also investigated how meridional and sagittal focusing with mirrors and bent crystals, respectively, introduce strong distortions in the wavefront, especially at the focal position.

The article is organized as follows. In §2 we give a theoretical introduction to the complex coherence factor and its particular definition in synchrotron sources. In §3 we briefly describe the experimental details of the measurements with the double-grating interferometer and the different configurations of the optical elements of the beamline which were studied. §4 shows measurements of the complex coherence factor recorded using a pseudo-channel-cut and a double-crystal monochromator. In §5 the wavefront analysis after different optical elements is shown; the comparison between the two monochromators and the study of the wavefront as a function of focusing. The results of all previous measurements are presented in §6 and a discussion in the context of a coherent diffraction experiment is elaborated in §7. Finally, conclusions are given in §8.

2. Theoretical background

Synchrotron undulators are chaotic X-ray sources emitting in a broad energy spectrum. Therefore, the transverse coherence length at a certain distance from the source and at a certain wavelength is given essentially by the size of the source and the longitudinal or temporal coherence is given by the bandwidth of the monochromator, which is usually a multilayer, a grating, a crystal or set of crystals placed after the source. In the following we assume that the beam is monochromatic and we will focus on the transverse coherence properties of the beam at the sample position, after passing through the monochromator.

We approximate the intensity distribution of an undulator source by a two-dimensional Gaussian distribution,

$$I(s_x, s_y) = I_0 \exp\left(-\frac{s_x^2}{2\sigma_x^2} - \frac{s_y^2}{2\sigma_y^2}\right), \quad (1)$$

where s_x and s_y denote the coordinates perpendicular to the optical axis at the source plane and σ_x and σ_y represent the size of the source in both directions. According to the van Cittert–Zernike theorem (Hecht, 2002), the complex degree of coherence or complex coherence factor (CCF) at the sample plane $|\gamma(x,y)|$ is given by the Fourier transform of $I(s_x,s_y)$. This results in another Gaussian distribution,

$$|\gamma(x, y)| = \gamma_0 \exp\left(-\frac{x^2}{2\xi_x^2} - \frac{y^2}{2\xi_y^2}\right), \quad (2)$$

provided that the extension of the distribution in the (x,y) plane is much smaller than the distance to the source, which is always the case at synchrotron beamlines. The parameters ξ_x and ξ_y are usually called transverse coherence lengths (r.m.s.) in the horizontal and vertical directions and they are related to the source size by

$$\xi_{x,y} = \lambda L/2\pi\sigma_{x,y}, \quad (3)$$

where λ denotes the wavelength and L is the distance between the source and the point of observation. The CCF is a normalization of the mutual intensity function, which gives correlations between two wavefields at different points of the sample plane. The optical elements in a beamline (slits, lenses, Be windows *etc.*) can degrade the coherence properties inherent to the undulator source. In the case of a defect in an optical element such as in a Be window, the beam is scattered and refracted by the defect, which acts as an effectively larger secondary source. In this situation it has been calculated that the CCF has two components: one preserves the coherence length given by the primary source [equation (3)] and the other has a smaller coherence length, arising from the secondary source caused by the defect (Vartanyants & Robinson, 2003). Such a CCF has also been measured after a defect on a diamond window (Pfeiffer *et al.*, 2005). However, not all optical elements cause this effect on the CCF. As we will show, vibrations of an optical element just decrease the coherence length owing to an effective larger source, provided that in the measurement one averages over a time larger than one period of the vibrations. In these cases, no component of the original source remains in the CCF.

3. Experimental set-up

Measurements were carried out at the ID01 beamline at the ESRF. This beamline has two monochromators which can be used alternatively: a pseudo-channel-cut monochromator (CCM) placed at a distance D = 30.4 m from the source (see Fig. 1*a*) and a double-crystal monochromator (DCM) placed at a distance D = 34.0 m from the source (see Fig. 1*b*). The CCM is a monolithic Si-111 crystal fabricated at the optics laboratory of the ESRF (Zhang *et al.*, 2003). It is made of a single piece of Si with a weak link between the two surfaces of the crystal, in such a way that it is possible to tilt the second surface with respect to the first one by mechanically pushing on it. In this way a small misalignment between the crystals is used to suppress higher-order harmonics. The DCM is made of two separate Si-111 crystals which move independently. The second crystal can be bent for sagittal focusing. This monochromator is frequently used in combination with two mirrors, as shown in Fig. 1(*b*). Each mirror consists of a single Si crystal of length 1 m. The first mirror M_1 helps to absorb the heat load from the white beam and it collimates the beam for optimum spectral resolution. Both mirrors can be bent, but in practice the first mirror M_1 is usually kept flat and only the second mirror M_2 is bent for meridional focusing.

The configuration of the DCM is preferred for high-flux experiments because of its focusing capability and it has the advantage of a high rejection efficiency of higher harmonics by the mirrors. However, such a monochromator is very sensitive to vibrations introduced by the liquid-N_2 cooling system and, as a result, the beam fluctuates at the sample position with oscillations of a few tens of micrometers. The pumping frequency of the liquid N_2 is about 50 Hz. On the other hand,

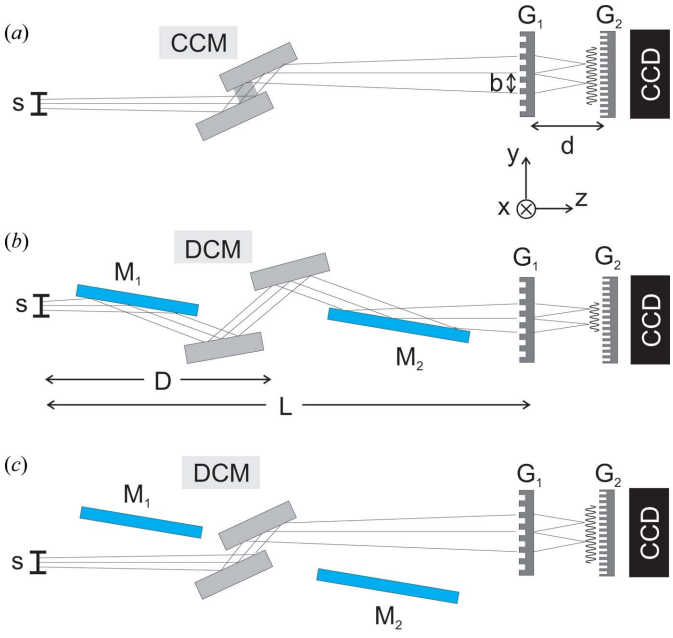

Figure 1
Double-grating interferometer set-up in the two possible configurations with the pseudo-channel-cut monochromator (CCM) (*a*) and the double-crystal monochromator (DCM) (*b*). While the DCM can be used with (*b*) or without mirrors (*c*), the CCM can only be used without them owing to beam-path constraints.

the CCM configuration provides a very stable beam within 2 µm at the sample position. As we will show below, it is due to this stability that the coherence properties of the beam are better preserved using the CCM.

We performed our measurements with a double-grating interferometer (Pfeiffer *et al.*, 2005). As shown in the sketch of Fig. 1, the set-up consisted of a phase grating G_1 with a period p_1 of a few micrometers which split the incoming beam mainly into the +1 and −1 diffraction orders. The diffracted beams interfered downstream, producing an interference pattern with a period which is equal to $p_1/2$. A second absorption grating G_2 with a period $p_2 = p_1/2$ was placed downstream, producing a moiré fringe pattern with a period of the order of hundreds of micrometers. The moiré fringe pattern can be easily detected with conventional X-ray detectors. This interferometer detects the first derivative of the phase of the wavefront with respect to y and it can be used for wavefront analysis (Weitkamp, Nöhammer *et al.*, 2005), quantification of the coherence (Pfeiffer *et al.*, 2005) and phase-contrast imaging (Weitkamp, Diaz *et al.*, 2005). In this experiment we took advantage of its two first functionalities, which are well described in the literature cited above. In the following we briefly describe our experimental set-up.

The phase grating G_1, made of Si, had a period $p_1 = 4$ µm and a thickness of 15.5 µm, designed for an optimal diffraction efficiency at an energy of 12.1 keV. It was placed at the sample position at the center of a diffractometer, at a distance L = 48.2 m from the source. The absorption grating G_2, consisting of Au lines, had a period $p_2 = 2$ µm and a thickness of 12 µm, and was fixed in front of the detector. Details of the gratings' fabrication can be found by David *et al.* (2007). The detector was installed on a translation stage after the diffractometer and it could move along z in such a way that the distance d between G_1 and G_2 ranged from 0.02 to 3 m. As a detector we used an Andor CCD (iXon DU885) with 1004 × 1002 pixels coupled to a LAG:Eu scintillator of thickness 12 µm by an optical lens with a magnification factor of ×4. The effective pixel size of the CCD was 2 µm taking into account the magnification of the lens. The resolution of the detector system was determined by a point spread function of about 3 µm. In all our measurements we used an energy of 13 keV and a single U35 undulator with a total length of 1.6 m. The gap of the undulator was set to 15 mm. The beam size was determined by slits placed in front of the monochromators with an opening of 1.5 mm × 1.5 mm. Under these conditions the heat load on the monochromator was below 400 W and therefore no strong distortions were expected in the crystals (Zhang *et al.*, 2003; Chumakov *et al.*, 2004). CCD frames were taken with an exposure time of 20 ms.

4. Measurement of the CCF

For the measurement of the CCF we recorded different moiré fringe patterns at several distances d between the two gratings. At every distance d, interference occurs between two beams which are separated by a distance $b = 2d\lambda/p_1$ at the position of G_1 (see Fig. 1). Therefore, the visibility of the moiré fringes as a function of b is a measurement of the CCF (Pfeiffer *et al.*, 2005). The visibility V is defined as

$$V = \frac{I_{\max} - I_{\min}}{I_{\max} + I_{\min}}, \tag{4}$$

where $I_{\max}$ and $I_{\min}$ denote the maximum and minimum intensity of a moiré fringe, respectively. From each interferogram recorded with the CCD, we analyzed the visibility by extracting the relevant Fourier component of the moiré fringe pattern. This analysis disregards any other feature in the intensity pattern recorded by the detector except for the moiré fringes themselves. However, this is perfectly justified because the moiré fringes are the only relevant feature in the measurement of the CCF (Pfeiffer *et al.*, 2005).

We performed two measurements, one using the CCM configuration (Fig. 1*a*) and the other with the DCM (Fig. 1*c*). Both mirrors M_1 and M_2 were removed from the beam in order to compare the coherence properties between both monochromators. As shown in Fig. 1, with the lines of the gratings oriented along the x direction, we measured the CCF along the vertical direction y. By rotating both G_1 and G_2 by 90° around the z axis, we then measured the CCF along the horizontal direction x for both CCM and DCM.

At first the grating lines were oriented as shown in Fig. 1 in order to measure the CCF along the vertical direction. In Fig. 2 we show a measurement of the visibility of the moiré fringes as functions of d on the top axis and b on the bottom axis. We show in blue the measurement with the CCM and in red that with the DCM. We observe that the visibility oscillates giving maxima at distances $d_n = np_1^2/8\lambda$, with n being an odd integer number (Weitkamp *et al.*, 2004) owing to the well known

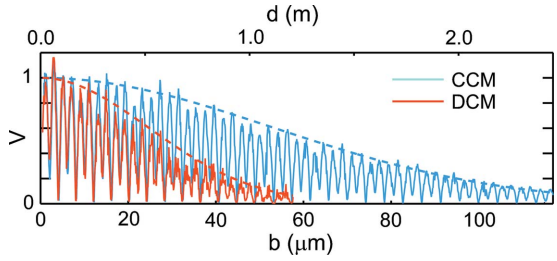

Figure 2
Measured visibility of the moiré fringe pattern as a function of the distance d between the two gratings (top axis) and the beam separation b at the position of the first grating (bottom axis). The lines of the gratings were oriented along the horizontal direction. We show in blue the measurement with the CCM and in red that with the DCM. The envelope functions were fitted to Gaussian curves (dashed lines) and they are a measurement of the complex coherence function in the vertical direction.

Talbot effect. More important for us are the envelope functions $V(b)$, which give a direct measurement of the CCF, *i.e.* the identification $V(b) = |\gamma(y)|$ can be done (Hecht, 2002; Pfeiffer *et al.*, 2005). We observe that the maxima of Talbot visibility fit well to Gaussian curves (dashed lines), as expected for a synchrotron source. The fitting parameters were γ_0 and ξ_y in equation (2) and the data were normalized to γ_0. The resulting transverse coherence length for the CCM was ξ_y = 53 μm, a factor 2.1 larger than for the DCM, which was ξ_y = 25 μm.

We then rotated G_1 and G_2 by 90° in order to measure the CCF along the horizontal direction. The measurements are not shown here but they resemble those of Fig. 2, with the exception that their corresponding envelope curves decay faster owing to the larger source size in the horizontal direction. In Tables 1 and 2 we show a summary of the measured transverse coherence lengths ξ (Table 1) and effective r.m.s. source sizes σ (Table 2) for both monochromators in both directions. The σ values were obtained from ξ according to equation (3). The expected source sizes given by the machine group of the ESRF are also given in Table 2. Discrepancies between measured and expected values are discussed in §6.

5. Wavefront analysis

For wavefront characterization, we placed G_1 at the sample position and G_2 at a distance d = 106 mm corresponding to a maximum of Talbot visibility. Interferograms with many moiré fringes were recorded and analyzed as described elsewhere (Weitkamp, Nöhammer *et al.*, 2005). In order to obtain many moiré fringes, G_1 is rotated by a small angle around the z direction (typically between 1° and 2°) using a motorized goniometer. From a given moiré fringe pattern, it is possible to measure the local wavefront radius of curvature R at the sample position by

$$R = \frac{a_m}{p_2} \frac{d}{\tan \theta_m}, \qquad (5)$$

where θ_m is the tilting angle of the fringes and a_m is the spacing between fringes. We show in Fig. 3(*a*) an example of a moiré fringe pattern recorded with the CCM and the lines of G_1 and

Table 1
Measured transverse coherence length ξ (r.m.s.) in μm.

Direction	CCM	DCM
Vertical	53 ± 1	25 ± 1
Horizontal	11 ± 1	7.1 ± 0.5

Table 2
Measured and expected source size σ (r.m.s.) in μm.

Direction	CCM	DCM	Machine
Vertical	13.8 ± 0.3	30 ± 1	10.3
Horizontal	64 ± 7	102 ± 7	57

G_2 oriented along the x direction (note that the method is sensitive to the local wavefront radius of curvature in the direction perpendicular to the lines of G_1 and G_2). In this interferogram we observe horizontal stripes of varying intensity, probably arising from insufficient polishing of the crystal surfaces of the monochromator. More interesting for us are the vertical moiré fringes, which provide an indication of the wavefront distortions. The image of the beam recorded without interferometer would look exactly the same as Fig. 3(*a*) but without the moiré fringes. These fringes become clearer after extracting the relevant Fourier component from the interferogram, as shown in Fig. 3(*b*). We then calculate the local wavefront radius of curvature according to equation (5)

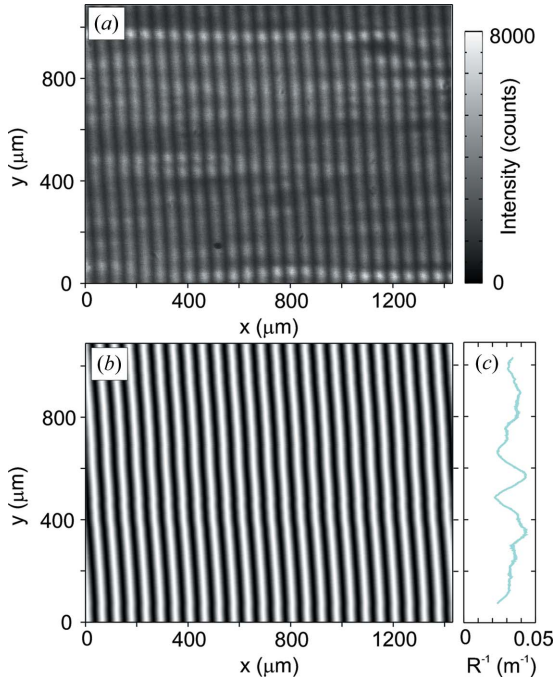

Figure 3
(*a*) Interferogram recorded at a distance corresponding to a maximum of Talbot visibility with the CCM. The interferometer gratings were set in such a way that their lines were oriented along the x direction. (*b*) Extraction of the relevant fringes from the interferogram shown in (*a*). (*c*) Local wavefront radius of curvature (abscissa) extracted from the interferogram in (*b*). The method used provides a value for the local wavefront radius of curvature at each y position averaged over the entire size of the image in (*b*) along the x direction.

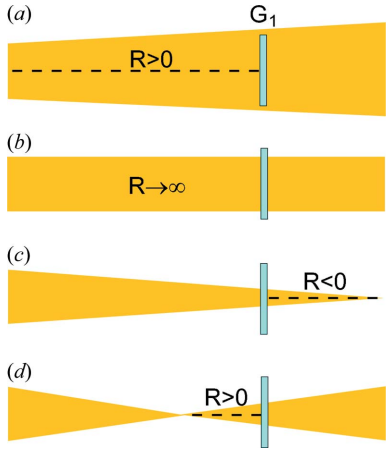

Figure 4
Convention for the sign of the radius of curvature: $R > 0$ for a divergent beam and $R < 0$ for a convergent beam at G_1. The beam can be naturally divergent (*a*), parallel (*b*), focused after G_1 (*c*) or focused before G_1 (*d*).

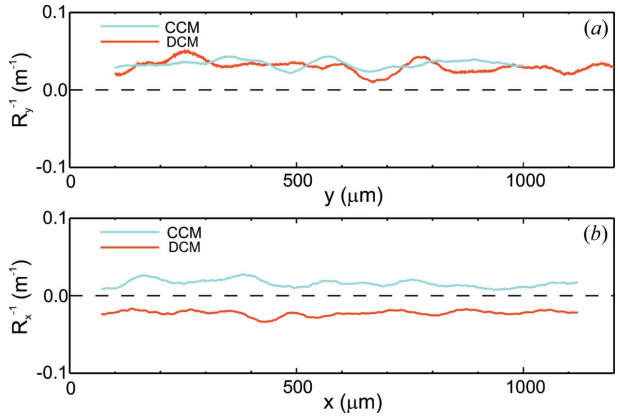

Figure 5
Comparison of the local wavefront radius of curvature at the sample position with the CCM (blue lines) and with the DCM (red lines). We show in (*a*) measurements of the vertical radius of curvature R_y and in (*b*) the horizontal radius of curvature R_x.

at each pixel position along the y direction and we average over the total number of fringes along the x direction (25 fringes in this example). In Fig. 3(*c*) we display the resulting wavefront analysis, with the measured inverse local wavefront radius of curvature in the vertical direction R^{-1} in the abscissa as a function of the pixel position along the y direction in the ordinate. As explained above, the method used provides a value for the local wavefront radius of curvature at each y position averaged over the entire size of the image in Fig. 3(*b*) along the x direction.

In order to analyze the wavefront in the horizontal direction, both gratings were rotated by an angle of 90° in the same way as for the measurement of the horizontal transverse coherence length in the previous section. In general, when analyzing the wavefront curvature in one direction, the respective perpendicular direction is averaged over the entire detector size. Wavefront analysis with a high resolution in the other direction is possible by performing phase-stepping measurements (Weitkamp, Diaz *et al.*, 2005). Such an analysis is out of the scope of this work, in which we only aim for trends in the wavefront distortions after focusing elements. The wavefront radius of curvature R can be positive or negative depending on whether the beam is divergent or convergent at the position of G_1. In Fig. 4 we show the convention for the sign of R and the four different cases which we will encounter in the analysis. The sign of R can be chosen depending on how we define the sign of the relative rotation between G_1 and G_2, which determines the tilting direction of the fringes (*i.e.* the sign of θ_m) in the interferogram.

5.1. Comparison between monochromators

For the wavefront analysis along the vertical direction (y direction), the lines of G_1 and G_2 were oriented along the x direction as shown in Fig. 1. We recorded two interferograms with an exposure time of 20 ms using the CCM and the DCM without mirrors, in order to compare both monochromators. The inverse of the measured wavefront radius of curvature in the vertical direction R_y^{-1} is shown in Fig. 5(*a*) (blue line) as a function of the position y. For comparison, the measured R_y^{-1} with the DCM is shown (red line). In both cases we observe similar wavefront distortions with an average radius of curvature of about 30 m and variations between 25 and 50 m. According to our convention (Fig. 4), the positive sign of R_y indicates that the beam is divergent at the sample position, as expected. However, we expect an average radius of curvature of 48 m, corresponding to the distance L between the source and G_1. This discrepancy might be due to imperfections in the crystal, as suggested by the horizontal intensity stripes observed in Fig. 3(*a*).

Many other interferograms were taken in order to check the reproducibility of our measurements. In the case of the CCM, they yielded almost identical wavefront profiles as that shown in Fig. 5(*a*). Because of the vibrations existing in the DCM set-up, different measurements resulted in different wavefront profiles. However, the minimum, maximum and average values of R_y did not change significantly. In the analysis, both the tilting angle of the fringes θ_m and the resulting radius of curvature R_y have been smoothed in order to consider the slow variations of the wavefront only. It is not our aim to measure a high-resolution map of the wavefront curvature, but to follow its trends over a length scale which is larger than the resolution in the measurement.

The results of the wavefront analysis in the horizontal direction are shown in Fig. 5(*b*), for which the gratings were rotated by an angle of 90° around the beam direction. The most striking result is that the beam is horizontally convergent when using the DCM. This is due to a residual sagittal focusing in the second crystal of the DCM. Owing to mechanical constraints in the set-up of the crystal, it is not possible to set it completely flat. This effect was suspected from indirect measurements such as the focal spot size of the beam after focusing with Be compound refractive lenses. With the double-grating interferometer we directly measured that the wavefront curvature is convergent at the sample position. For the

CCM, the horizontal wavefront radius of curvature R_x has an average value of 50 m, as expected from the distance to the source, and variations between 33 and 100 m.

5.2. DCM with mirrors

The comparison between monochromators shown above reveals no substantial difference in wavefront distortions when using the CCM and the DCM without mirrors. However, the DCM is typically used with mirrors because the heat load on the first crystal causes drifts and instabilities in the beam (note that up to three undulators can be simultaneously used at this beamline). This is not a problem for the CCM, in which a recently developed cooling system allows its operation without mirrors. In the following we show a wavefront analysis using the DCM with mirrors, as sketched in Fig. 1(*b*). The focusing capability of the second mirror M_2 in the vertical direction (meridional focusing) and of the second monochromator crystal in the horizontal direction (sagittal focusing) allows for a study of the wavefront distortions as a function of the focus in both directions. Focusing will not only drastically change the wavefront radius of curvature but, as will be shown, it will also introduce large distortions in the wavefront.

The measurements of the wavefront radius of curvature in the vertical direction R_y are shown in Fig. 6(*a*) for different radius of curvature of the mirror R_m. We observe that the extension of the beam along the vertical direction of the detector y changes for different focusing values, as the beam size at the position of G_1 changes owing to the focusing. The black line corresponds to the measurement without mirrors shown in Fig. 5(*a*) in red. With R_m = 28 km, the average wavefront radius of curvature is very large, as expected for a quasi-parallel beam, but the oscillations indicate strong local wavefront distortions at the sample position. We believe that these distortions arise from imperfections in the mirrors which are clearly visible in the intensity recorded by the CCD without the interferometer. For R_m = 11 km we observe a decrease of the size of the beam accompanied by an increase of local distortions. The average radius of curvature is negative, as expected for a convergent beam which is focused after G_1 (see Fig. 4*c*). When the beam is focused at the position of G_1 (R_m = 6.9 km) a very high intensity is recorded on the CCD over a range of about 200 µm in the y direction, corresponding to the range of the curve shown in Fig. 6. However, the wavefront analysis shows enormous distortions of the beam, which is diverging on average at low y values and converging at high y values. For even lower values of R_m, the beam is focused before G_1 and we observe a divergent wavefront corresponding to the situation sketched in Fig. 4(*d*).

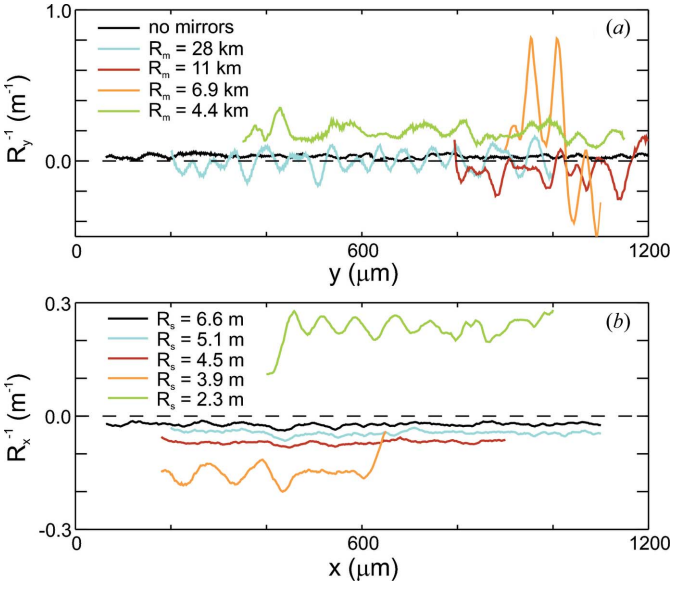

Figure 6
Wavefront radius of curvature using the DCM with mirrors in the vertical direction (*a*) and in the horizontal direction (*b*). Different colors correspond to different curvatures of the second mirror M_2 in (*a*) and the second monochromator crystal in (*b*). Details are given in the text.

In the horizontal direction the wavefront radius of curvature R_x was studied as a function of the radius of curvature R_s of the second crystal of the DCM. Measurements of R_x are shown in Fig. 6(*b*). In all these measurements, M_2 was kept at R_m = 28 km, for which we obtain a quasi-parallel beam in the vertical direction. The first measurement was performed at R_s = 6.6 m, which corresponds to the nominally unfocused beam in the sagittal direction. However, the measured negative R_x reveals a convergent beam, indicating that the radius of curvature of the crystal R_s at nominally zero focusing is clearly smaller than expected. For decreasing values of R_s, we observe that the illuminated part of the detector in the x direction diminishes and that the average (negative) radius of curvature R_x decreases, indicating that the focus approaches G_1. At the closest measured position of the focus to G_1 (R_s = 3.9 m), wavefront distortions appear. However, they are smaller than the distortions observed in the vertical direction at the maximum focus. Finally, at R_s = 2.3 m, the beam is focused before G_1 and a divergent beam is measured with similar distortions in the wavefront.

6. Results

In order to compare the measured source size with the expected values given by the machine group of the ESRF for a low-β section of the ring (see Table 2), we need to take into account the wavefront analysis presented above. In the vertical direction the average wavefront radius of curvature is approximately 33 m for both monochromators, while a radius of curvature of around 50 m is expected owing to the distance from the source to the measurement position. Since the monochromator is the only optical element present in these measurements, we attribute the smaller radius of curvature to imperfections in the monochromator crystals, as suggested by the intensity stripes observed in Fig. 3(*a*). More importantly, the coherence length is expected to scale with the beam divergence, creating an effective source size different from the real source size. Assuming an ideal source size of 10.3 µm and assuming a divergence of the beam like the one measured for

the CCM and the DCM, we can expect to measure an effective source size of 15 μm, which is very close to the measured value of 13.8 μm in the case of the CCM.

An increase in the vertical effective source size with the DCM by a factor of two can be explained by relative vibrations between the two crystals of the monochromator around the *x* axis. As shown by Weitkamp (2002), one can estimate the relative angular vibrations $\Delta\theta$ from the spread in source size with respect to the expected value by simple geometrical considerations. From our measurement we have estimated an angular amplitude of $\Delta\theta = 0.9$ μrad. On the other hand, CCMs are not so sensitive to vibrations because they are made of a single crystal. This is why, after taking divergence effects into account, the measured source sizes with the CCM are in fact very close to the expected values.

In the horizontal direction, the average wavefront radius of curvature is 50 m with the CCM, exactly as expected. Therefore the measured source size can be directly compared with the expected value and they are indeed very close (see Table 2). On the other hand, the average wavefront radius of curvature measured with the DCM reveals a convergent beam with an average radius of curvature of −50 m. Assuming a real source size with the expected r.m.s. value of 57 μm in the horizontal direction, one can estimate an effective source size of 104 μm owing to this focusing effect, which is very close to the source size measured in §4 (see also Table 2).

Effective larger sources have already been observed before in synchrotron beamlines and have usually been attributed to vibrations or other imperfections in the X-ray optical elements, without further experimental proof. Here we are able to distinguish, for the first time, between an increase in the effective source size caused by a change in the beam divergence and the same effect caused by relative vibrations between the monochromator crystals. In both cases the resulting CCF can be fitted by a single Gaussian, indicating that the average beam at the measurement point can be regarded as originating from a source with an effectively larger source size.

We note that the measured vertical coherence length is very large (53 μm r.m.s.) in spite of strong intensity oscillations along the vertical direction at similar length scales (see Fig. 3*a*). The CCF indicates the phase relation between incident beams at the measurement plane as a function of their distance *b* along the vertical direction (see Fig. 1*a*). Therefore, the intensity of the incoming beam is not relevant in the resulting coherence of the beam (van der Veen & Pfeiffer, 2004).

The analysis of the moiré fringes in Fig. 3 is introduced in order to asses the influence of the divergence of the beam for the interpretation of the resulting measured source size. Since the measurement of the CCF has been performed over the entire exposed detector area, only the average divergence over this area is relevant. Additionally, the fluctuations in the local wavefront radius of curvature along each direction allow for a qualitative study of the wavefront distortions, especially when analyzed as a function of focusing with the DCM (§5.2). In this case the averaging along the other direction is a feature of the method that we used. A resolved analysis in the other direction would be possible using the phase-stepping technique, as described by Weitkamp, Diaz *et al.* (2005). This method consists of the measurement of several moiré fringe patterns at different positions of G_1 with respect to G_2, in such a way that the change in position is along the direction perpendicular to the grating lines and over a few periods of the interference fringes. The phase-stepping allows for the measurement of intensity oscillations at each pixel of the detector, enabling a resolved measurement of both the CCF and the wavefront radius of curvature. Such an experiment would enable imperfections in the incoming wavefront to be resolved and, eventually, to relate them to imperfections in the optical elements of the beamline.

The unexpected divergence of the beam in the vertical direction was attributed before to possible imperfections in the monochromator crystal. However, our coarse analysis of the wavefront local radius of curvature is not sufficient to prove it. Another possible interpretation for a change in the beam divergence could be the heat load on the first monochromator crystal, which could produce a curvature on the crystal and on the diffracted wavefront. However, a similar wavefront curvature should then be produced along the horizontal direction and we do not observe such an effect, at least in the CCM.

Other methods different from the double-grating interferometer have been developed for the measurement of the source size at synchrotron sources (Kohn *et al.*, 2000; Guigay *et al.*, 2004; Leitenberger *et al.*, 2004) and for the measurement of the CCF (Lin *et al.*, 2003). The main advantage of the double-grating interferometer lies in the simultaneous measurement of the CCF and the beam divergence, which helps to determine the possible reasons for effectively larger source sizes.

7. Discussion

In this section we discuss the main results of our measurements in the context of a CDI experiment performed on a small (∼1 μm) strained crystal. Such a sample can be considered as a complex object in which the magnitude is given by its electron density distribution and its phase is related to the atomic displacements within the crystal (Takagi, 1969). The first requirement for a coherent diffraction experiment is that the sample is smaller than the coherence volume of the incoming radiation. This condition is easily fulfilled in synchrotron sources using a Si 111 monochromator. However, if the incoming radiation has a distorted wavefront, distortions will add to the phase of the complex object and the retrieved phase in a CDI experiment will show a superposition of the wavefront distortions onto the displacement field within the crystal. Therefore, it is important to choose optical elements which minimize the wavefront distortions at the sample position.

Another important issue in CDI experiments concerns the resolution achieved in the reconstructed image. It is a natural consequence of discrete Fourier transformations that the pixel size in the reconstructed image is given by $2\pi/\Delta$, where Δ denotes the range measured in reciprocal space. In order to

experimentally access a large q-range in reciprocal space, it is necessary to increase the flux incident onto the sample, for which focusing optics such as mirrors or lenses are generally used. In summary, it is necessary to find a compromise between high flux, high coherence and low wavefront distortions in CDI experiments. Here we attempt to discuss the optimal conditions for such experiments from the results shown above.

One of the most important results of our study is that vibrations in the monochromator increase the effective source size and they consequently cause a reduced transverse coherence length at the sample position. Additionally, the presence of mirrors in the DCM configuration (see Fig. 1*b*) increases the wavefront distortions at the sample position. Therefore, the pseudo-channel cut is the monochromator of choice at beamline ID01 for CDI experiments.

Focusing the beam has two important consequences. First, we expect a reduction of the transverse coherence length which, however, does not modify the shape of the CCF, as shown in §4 for the DCM in the horizontal direction. On the other hand, the effect of focusing on the wavefront distortions was studied in §5.2 using a focusing mirror. We found that wavefront distortions increase for larger bending values of the mirror and they become especially bad close to the focal plane. For these two reasons, special care must be taken in the interpretation of CDI results when tight focusing of X-rays is used.

It has been recently shown that focusing in the diffraction limit (using a coherent illumination of the lens) produces an X-ray focused spot which has a coherence length larger than the size of the spot, enabling CDI experiments (Robinson *et al.*, 2003; Schroer *et al.*, 2008). Additionally, the phase of the wavefront at the focal plane is expected to be approximately constant and well defined over a certain region within the focal spot. This has been confirmed in a recent experiment with a focused X-ray beam using ptychographic iterative methods (Thibault *et al.*, 2008), in which it is possible to retrieve both the wavefield scattered by the sample and the wavefield of the incident beam at the sample position. In order to produce a diffraction-limited focused spot, coherent illumination of the aperture of the focusing element is required. For this purpose, optics with no mechanical vibrations like the CCM are preferable, since they provide larger transverse coherence and therefore they allow for a higher coherent flux. This method seems to be the most efficient way to perform CDI on small single crystals with a high spatial resolution (Schroer *et al.*, 2008; Diaz *et al.*, 2009). There are cases, however, in which many identical crystals with the same orientation can be simultaneously illuminated with a coherence length which is larger than each individual crystal but smaller than the average distance between neighboring crystals. Under such conditions the ensemble average diffraction signal is an incoherent superposition of the coherent diffraction pattern from each individual crystal and CDI experiments can be performed (Zozulya *et al.*, 2008) in which the DCM with mirrors provides the appropriate coherence length.

8. Conclusion

We have quantified the coherence and wavefront distortions at a synchrotron radiation beamline after several optical elements such as a monolithic pseudo-channel-cut monochromator (CCM), a double-crystal monochromator (DCM) and mirrors using a double-grating interferometer. We measured a slightly larger divergence than expected in the vertical direction with both monochromators, possibly owing to defects in the monochromator crystals. We also found that the DCM causes an increase of the effective source size by a factor of two in both directions owing to mutual vibrations between the monochromator crystals in the vertical direction and to a residual focusing of the second crystal in the horizontal direction. The use of focusing mirrors, typically used in combination with the DCM, introduces strong wavefront distortions at the sample position. Our studies enable the choice of optical elements for different coherent diffraction experiments depending on the degree of coherence and the flux required.

In the future we would like to use the double-grating interferometer for the two-dimensional wavefront characterization after focusing lenses (Engelhardt *et al.*, 2007). Forward propagation of the wavefield will then enable imaging of the wavefront at the focal spot. This wavefront characterization is mandatory for the CDI of atomic displacement fields within nanocrystals, in order to separate the part of the phase arising from the wavefront in the reconstructed object phase.

We would like to thank staff at the ESRF ID01 beamline for technical support, Eric Ziegler for providing the gratings, and Anatoly Snigirev and Irina Snigireva for fruitful discussions. This work was partially funded by FWF, Vienna (SFB025 IR-On).

References

Abbey, B., Nugent, K. A., Williams, G. J., Clark, J. N., Peele, A. G., Pfeifer, M. A., de Jonge, M. & McNulty, I. (2008). *Nat. Phys.* **4**, 394–398.

Chumakov, A., Rüffer, R., Leupold, O., Celse, J.-P., Martel, K., Rossat, M. & Lee, W.-K. (2004). *J. Synchrotron Rad.* **11**, 132–141.

David, C., Bruder, J., Rohbeck, T., Grünzweig, C., Kottler, C., Diaz, A., Bunk, O. & Pfeiffer, F. (2007). *Microelectron. Eng.* **84**, 1172–1177.

Diaz, A., Mocuta, C., Stangl, J., Mandl, B., David, C., Vila-Comamala, J., Chamard, V., Metzger, T. H. & Bauer, G. (2009). *Phys. Rev. B*, **79**, 125324.

Dierker, S. B., Pindak, R., Fleming, R. M., Robinson, I. K. & Berman, L. (1995). *Phys. Rev. Lett.* **75**, 449–452.

Engelhardt, M., Baumann, J., Schuster, M., Kottler, C., Pfeiffer, F., Bunk, O. & David, C. (2007). *Rev. Sci. Instrum.* **78**, 093707.

Guigay, J.-P., Zabler, S., Cloetens, P., David, C., Mokso, R. & Schlenker, M. (2004). *J. Synchrotron Rad.* **11**, 476–482.

Gutt, C., Ghaderi, T., Chamard, V., Madsen, A., Seydel, T., Tolan, M., Sprung, M., Grübel, G. & Sinha, S. K. (2003). *Phys. Rev. Lett.* **91**, 076104.

Gutt, C., Sprung, M., Fendt, R., Madsen, A., Sinha, S. K. & Tolan, M. (2007). *Phys. Rev. Lett.* **99**, 096104.

Hecht, E. (2002). *Optics.* New York: Addison-Wesley.

Kohn, V., Snigireva, I. & Snigirev, A. (2000). *Phys. Rev. Lett.* **85**, 2745–2748.
Leitenberger, W., Wendrock, H., Bischoff, L. & Weitkamp, T. (2004). *J. Synchrotron Rad.* **11**, 190–197.
Lin, J. J. A., Paterson, D., Peele, A. G., McMahon, P. J., Chantler, C. T., Nugent, K. A., Lai, B., Moldovan, N., Cai, Z., Mancini, D. C. & McNulty, I. (2003). *Phys. Rev. Lett.* **90**, 074801.
Miao, J., Charalambous, P., Kirz, J. & Sayre, D. (1999). *Nature (London)*, **400**, 342–344.
Pfeifer, M. A., Williams, G. J., Vartanyants, I. A., Harder, R. & Robinson, I. K. (2006). *Nature (London)*, **442**, 63–66.
Pfeiffer, F., Bunk, O., Schulze-Briese, C., Diaz, A., Weitkamp, T., David, C., van der Veen, J. F., Vartanyants, I. & Robinson, I. K. (2005). *Phys. Rev. Lett.* **94**, 164801.
Robinson, I. K., Pfeiffer, F., Vartanyants, I. A., Sun, Y. & Xia, Y. (2003). *Opt. Express*, **11**, 2329–2334.
Schroer, C. G., Boye, P., Feldkamp, J. M., Patommel, J., Schropp, A., Schwab, A., Stephan, S., Burghammer, M., Schöder, S. & Riekel, C. (2008). *Phys. Rev. Lett.* **101**, 090801.
Shpyrko, O. G., Isaacs, E. D., Logan, J. M., Feng, Y., Aeppli, G., Jaramillo, R., Kim, H. C., Rosenbaum, T. F., Zschack, P., Sprung, M., Narayanan, S. & Sandy, A. R. (2007). *Nature (London)*, **447**, 68–71.
Takagi, S. (1969). *J. Phys. Soc. Jpn*, **26**, 1239–1253.
Thibault, P., Dierolf, M., Menzel, A., Bunk, O., David, C. & Pfeiffer, F. (2008). *Science*, **321**, 379–382.
Vartanyants, I. A. & Robinson, I. K. (2001). *J. Phys. Condens. Matter*, **13**, 10593–10611.
Vartanyants, I. A. & Robinson, I. K. (2003). *Opt. Commun.* **222**, 29–50.
Veen, F. van der & Pfeiffer, F. (2004). *J. Phys. Condens. Matter*, **16**, 5003–5030.
Weitkamp, T. (2002). *Imaging and Tomography with High Resolution Using Coherent Hard Synchrotron Radiation.* Göttingen: Cuvillier Verlag.
Weitkamp, T., Diaz, A., David, C., Pfeiffer, F., Stampanoni, M., Cloetens, P. & Ziegler, E. (2005). *Opt. Express*, **13**, 6296–6304.
Weitkamp, T., Diaz, A., Nöhammer, B., Pfeiffer, F., Rohbeck, T., Cloetens, P., Stampanoni, M. & David, C. (2004). *Proc. SPIE*, **5535**, 137–142.
Weitkamp, T., Nöhammer, B., Diaz, A., David, C. & Ziegler, E. (2005). *Appl. Phys. Lett.* **86**, 054101.
Williams, G. J., Pfeifer, M. A., Vartanyants, I. A. & Robinson, I. K. (2003). *Phys. Rev. Lett.* **90**, 175501.
Williams, G. J., Quiney, H. M., Peele, A. G. & Nugent, K. A. (2007). *Phys. Rev. B*, **75**, 104102.
Zhang, L., Lee, W.-K., Wulff, M. & Eybert, L. (2003). *J. Synchrotron Rad.* **10**, 313–319.
Zozulya, A. V., Yefanov, O. M., Vartanyants, I. A., Mundboth, K., Mocuta, C., Metzger, T. H., Stangl, J., Bauer, G., Boeck, T. & Schmidbauer, M. (2008). *Phys. Rev. B*, **78**, 121304.